RESEARCH ARTICLE

Influence of Forest-Edge Flows on Scalar Transport with Different Vertical Distributions of Foliage and Scalar Sources

Yulong Ma[1] · Heping Liu[1] · Zhenqing Liu[2] · Chuixiang Yi[3] · Brian Lamb[1]

Abstract

Forest edges have significant impacts on flow dynamics and mass exchange across the forest–atmosphere interface. A better understanding of edge flows and scalar transport has implications for locating and interpreting eddy-covariance flux measurements over finite-size forests with edges. Here the large-eddy simulation module within the Weather Research and Forecasting model is deployed to study the influence of forest edges on flow dynamics and scalar transport for a range of vertical distributions of foliage and scalar sources/sinks. For plant canopies with a relatively dense trunk space, a strong in-canopy flow convergence develops near the leading edge, which dominates the flow dynamics and leads to distinct scalar concentration and flux patterns not only across edges but also across the forest–atmosphere interface for sources near the ground and lower part of the canopy. For plant canopies with a deep, sparse trunk space, a strong and long sub-canopy jet develops, leading to simpler features in flow dynamics and scalar transfer. A real case with scalar sources/sink distributions as simulated by a newly developed multiple-layer canopy module produces even more complex scalar concentration and flux patterns. The budget equations for scalars are also analyzed to quantify the contributions of different terms to scalar fluxes. Our results demonstrate that both the scalar source distributions and canopy structures should be considered when eddy-covariance flux measurements are made over finite-size forests with edges.

Keywords Forest canopy · Forest edge · Large-eddy simulations · Scalar transport · Weather Research and Forecasting model

✉ Heping Liu
  heping.liu@wsu.edu

1 Department of Civil and Environmental Engineering, Washington State University, Pullman, WA, USA

2 School of Civil Engineering & Mechanics, Huazhong University of Science and Technology, Wuhan, Hubei, China

3 School of Earth and Environmental Sciences, Queens College, City University of New York, New York, NY 11367, USA

1 Introduction

Forests cover about 30% of the land surface, playing an important role in biosphere–atmosphere exchanges of energy, water vapour, and trace gases (Bonan 2008). A variety of natural and human disturbances such as wildfires, logging, bark beetles, windthrow, and extreme weather events (Yi et al. 2015) create highly heterogeneous forested landscapes with edges, leading to highly spatially-heterogeneous flows (Yang et al. 2006; Dupont and Brunet 2008, 2009; Sogachev et al. 2008; Kanani-Sühring and Raasch 2015, 2017). It is well recognized that forest-edge effects pose significant problems when interpreting eddy-covariance measurements of the surface energy balance and carbon budgets over heterogeneous forested landscapes (Oldroyd et al. 2014; Foken et al. 2017). A better understanding of forest-edge flow dynamics and associated scalar transfer will offer insight into how to reduce uncertainty in eddy-covariance measurements over highly heterogeneous forested areas.

Efforts have been made to study forest-edge flows using analytical models (Belcher et al. 2003; Kröniger et al. 2017), large-eddy simulations (Yang et al. 2006; Dupont and Brunet 2008; Cassiani et al. 2008; Kanani et al. 2014; Kanani-Sühring et al. 2017), and field measurements (Klaassen et al. 2002; Schlegel et al. 2012; Foken et al. 2017). All studies demonstrate that forest edges substantially influence mean and turbulent flow dynamics, scalar transport, and the surface energy imbalance problem. Such forest-edge effects can be significant not only around the upwind and downwind edges but also in a region extending from the edge to a great downwind distance in both horizontal and vertical dimensions, depending on leaf area index (LAI) and inflow dynamics (e.g., Klaassen et al. 2002; Dupont and Brunet 2008; Belcher et al. 2012).

The vertical foliage distributions have a significant impact on the edge-flow features (Cassiani et al. 2008; Dupont et al. 2012; Kanani-Sühring and Raasch 2015). Forest edges with a relatively dense trunk space and $LAI > 5 \, \mathrm{m^2 \, m^{-2}}$ are likely to lead to the development of an in-canopy recirculation at some distance from the leading edge (Kanani-Sühring and Raasch 2015). Such an in-canopy recirculation can also develop below canopy with a vertically uniform foliage once $LAI \gtrsim 4 \, \mathrm{m^2 \, m^{-2}}$. However, this in-canopy recirculation rarely develops near a forest edge with most of its foliage distributed at the upper part of trees and a deep, sparse trunk space at the lower part, such as maritime pine (Dupont et al. 2011). Nevertheless, this deep, sparse trunk space allows a strong sub-canopy jet with high turbulence kinetic energy (TKE) to develop across a great distance from the leading edge. In contrast, a sub-canopy jet is less pronounced for forests with a relatively dense trunk space and uniformly distributed foliage. Although these edge flow dynamics associated with the vertical foliage distributions have been reported in the literature, their impacts on scalar transport remain less studied.

In canopies with a relatively dense trunk space and with uniformly distributed foliage and uniform sources, flow convergence downwind of the leading edge results in an increased scalar concentration and enhanced fluxes (Sogachev et al. 2008; Yi 2008; Ross and Baker 2013; Kanani-Sühring and Raasch 2015, 2017). Dupont et al. (2011, 2012) found that the flow patterns are remarkably different in the lower layers of a maritime pine forest with a deep, sparse trunk space. Ross and Harman (2015) have demonstrated that the effect of scalar source distribution on scalar transport is significant over a forested hill. However, the scalar transport and distributions within a maritime pine forest remain less understood. Also, the impacts of different source distributions on scalar transport over a forest edge are less investigated. Another limitation is that the forest patch length is relatively short (e.g.,

about 30 times the canopy height), which remains unclear as to whether such conclusions are applicable for forest-edge flows with long patch length.

Here we investigate (i) the influences of three different vertical foliage distributions on upwind and downwind forest-edge flow dynamics and associated spatial variations in mean concentration and fluxes under neutral atmospheric stability conditions; and (ii) the influences of scalar source distributions on the scalar transport under forest-edge flows. We choose three widely identified plant canopies with three types of vertical foliage distributions which are represented in our model as uniformly distributed foliage, a canopy with a relatively dense trunk space and a canopy with a deep and sparse trunk space (Fig. 1). To address these two objectives, we deploy the Weather Research and Forecasting (WRF) model with the large-eddy simulation module (the WRF–LES model; Skamarock et al. 2008) including a new multiple-layer canopy module (hereafter the MCANOPY module) as described and evaluated in Ma and Liu (2019). The MCANOPY module is largely based on the framework of the Community Land Model version 4.5 (CLM4.5; Oleson et al. 2013), taking into account all important physical and physiological canopy processes. The MCANOPY module and the simulation configurations are described in Sect. 2. Section 3 introduces the edge flow dynamics, while Sect. 4 discusses scalar transport with a horizontally uniformly distributed constant-flux ground source with identical flows. Section 5 examines the linkages of spatial variations in concentration and fluxes to scalar sources located in different canopy layers with identical flows. In Sect. 6, a fully coupled run with the WRF–LES–MCANOPY model is conducted to investigate the CO_2 and water vapour transport over a forest edge with the identical flows. The conclusions are provided in Sect. 7.

2 Numerical Methods

2.1 Model Description

The WRF–LES model version 3.9 is used (Skamarock et al. 2008). For the LES module, a low-pass filter operates on flow field variables to separate large eddies from small ones, where large eddies are explicitly resolved and small eddies are parametrized using a subgrid-scale (SGS) scheme. In the WRF–LES code, the grid spacing acts as an implicit filter. The WRF–LES model solves the filtered (space-averaged) momentum equation as

$$\frac{\partial \bar{u}_i}{\partial t} + \frac{\partial \bar{u}_i \cdot \bar{u}_j}{\partial x_j} = -\frac{1}{\rho}\frac{\partial \bar{p}}{\partial x_i} - \frac{\partial \tau_{ij}}{\partial x_j} + F_{u,i}, \tag{1}$$

where t is time, $\bar{u}_i$ is the filtered velocity in direction x_i ($x_1 = x$ represents streamwise direction, $x_2 = y$ represents spanwise direction, and $x_3 = z$ represents vertical direction), ρ is air density, $\bar{p}$ is the filtered pressure, and $F_{u,i}$ is the forcing term (e.g., the canopy drag force). In the LES model, τ_{ij} represents the sub-grid scale stresses, which are parametrized using the SGS scheme. Here the Lagrangian-averaged scale-dependent Smagorinsky model (Porté-Agel et al. 2000; Bou-Zeid et al. 2005) is chosen to parametrize the subgrid-scale stresses since this turbulence model shows promising performance in complex terrain (Ma and Liu 2017).

For the aerodynamic drag due to the canopy elements in the MCANOPY module, a porous body assumption is adopted for consistency with previous studies (e.g., Shaw and Schumann 1992). The canopy drag force is modelled as
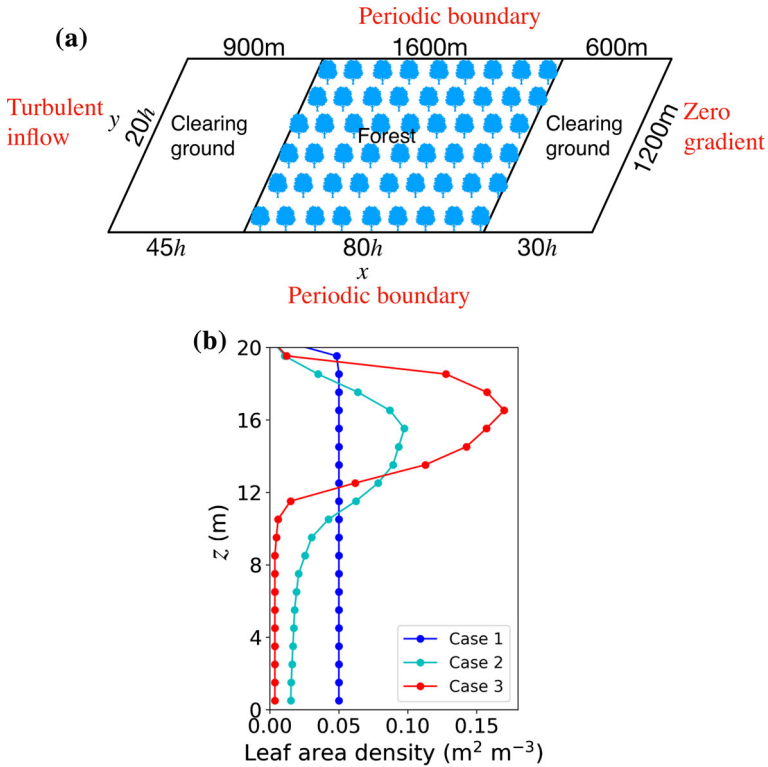
$$F_{u,i} = -c_d a |U| \bar{u}_i, \tag{2}$$

Fig. 1 a The simulation domain setting. **b** The leaf area density (*LAD*) profiles for the three simulation cases. The leaf area index (*LAI*), which is the height-integrated *LAD*, is identical for the three cases with a value of 4

where c_d is the forest drag coefficient (0.25), a is the leaf area density for each canopy layer, U is the local wind speed, $\bar{u}_i$ is the velocity component in the x_i-direction, and $F_{u,i}$ is the drag force that is added to the momentum equations.

In addition to the drag effect in a momentum drag module, a full suite of canopy processes is also parametrized in the MCANOPY module, including a two-stream radiative transfer module, a leaf energy balance module, a photosynthesis module, and a ground-surface energy balance module. The WRF–LES–MCANOPY model provides the within-canopy fluxes of momentum, heat, water vapour, and CO_2 thereby leading to changes in wind speed, air temperature, specific humidity, and CO_2 concentration in the canopy airspace, respectively. A detailed description and validation of the MCANOPY module and the WRF–LES–M-CANOPY model are summarized elsewhere (Ma and Liu 2019). These new features of the MCANOPY module and its fully coupled operation with the WRF–LES–MCANOPY model allow more realistic studies about the influence of canopy-edge flows on scalar transport.

2.2 Simulation Configurations

All the simulations presented here are performed over a rectangular domain in Cartesian coordinates with u, v, and w representing the velocity components in the streamwise, span-wise, and vertical directions, respectively. A domain size of 3.1 km × 1.2 km × 0.2 km in the

x, y, and z directions is used, as shown in Fig. 1a, same as that of Dupont et al. (2012). The horizontal grid resolution is 3 m, and the vertical resolution is 1 m within the canopy (below 20 m) and stretched above with a 7.5 m grid spacing at the domain top. The surface roughness length is set to be 0.1 m. At the top of the domain, a rigid boundary is used by setting the vertical velocity to zero, and a free-slip boundary is used for horizontal velocities and stresses. A Rayleigh damping layer is applied at the top with a height of 30 m. Fifth- and third-order upwind-biased spatial-differencing methods are deployed for solving the horizontal and vertical advection terms, respectively. For all the simulations, the flow is driven by a constant pressure-gradient force in the streamwise (x) direction and the Coriolis effects are neglected. To keep the same inflow conditions for all runs, the turbulent inflow field is generated with the precursor simulation method in which simulations with the periodic boundary conditions are made over the same domain but on a flat rough ground without forests. Once the flow reaches a statistically-stationary state and the turbulence is fully developed, the velocity data (u, v, and w) are extracted from a y–z plane and then stored at each timestep (0.03 s). The turbulent inflow is enforced at the western lateral boundary and a zero-gradient boundary at the eastern boundary. The northern and southern boundaries are treated by the periodic boundary conditions, as in Ma and Liu (2017).

For all the runs, the canopy height (h) is set as 20 m, the plant canopy is divided into 20 sub-layers, and the canopy $LAI = 4$ m^2 m^{-2}. Three leaf area distributions are considered, including the uniformly distributed (case 1), the one with a relatively dense trunk space (case 2), and the one with dense crown layers and a sparse trunk space (case 3), as shown in Fig. 1b. The forested patch covers the length of $80h$ in the middle of the domain in the x-direction and the entire y-direction (Fig. 1a). Two treatments of the scalar source distributions are adopted in our simulations. The first treatment considers the horizontally uniformly distributed constant flux sources at the rate of 1 μmol m^2 s^{-1} released at the forested ground, the cleared cut ground, and the canopy sub-layers at the heights of $0.3h$, $0.6h$, and $0.9h$, similar to the source treatment in Ross and Harman (2015). The background scalar concentration is set to be 100 μmol m^{-3}. The second set of treatment considers CO_2 sources/sinks and specific humidity (H_2O) sources calculated directly by the MCANOPY module in WRF–LES–MCANOPY coupled runs, which is considered to be a more realistic case.

After the flow reaches its steady state, the turbulence fluctuations are defined as the departures from the spanwise space-averaged values at each height, denoted by the symbol prime ($'$). The statistical quantities shown in the figures are calculated using a space- (y-direction) and time-averaging procedure, which is denoted by the symbol $\langle \ \rangle$. The time–averaging is performed over 160 instantaneous samples collected every 5 s during a 30-min period.

3 Edge Flow Dynamics Associated with Three Types of Leaf Area Density Profiles

Major forest-edge flow features summarized in Dupont and Brunet (2008) and Belcher et al. (2012) are reproduced well by our model system (Fig. 2). As the flow approaches the leading edge, wind speeds are reduced in this impact region (x/h from 0 to 5) due to the increased pressure induced by the forest. The flow penetrating into the forest creates a sub-canopy jet extending from the leading edge to a certain distance downwind. As compared with case 1 and case 2, the sub-canopy jet is more pronounced in case 3 with the relatively sparse foliage at the lower part of the canopy, suggesting that its intensity and persistence-length
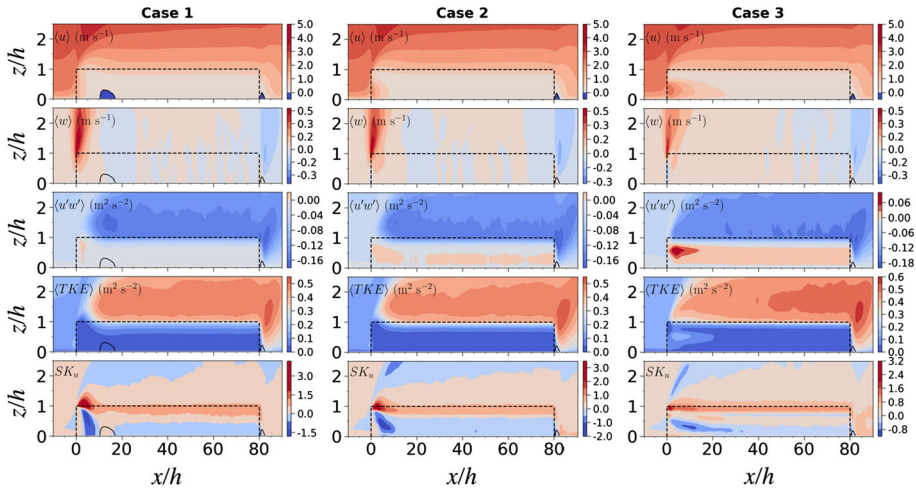
Fig. 2 Forest-edge flow dynamics associated with the three different vertical distributions of foliage as shown in Fig. 1. The dashed black line denotes the forest. For each case, the panels from top to bottom show the averaged streamwise velocity u, vertical velocity w, momentum flux $u'w'$, turbulence kinetic energy TKE, and streamwise velocity skewness SK_u. All quantities are spatially averaged in the y direction and then time-averaged

are largely dependent on the foliage distribution (Cassiani et al. 2008). Note that an in-canopy recirculation with a negative-velocity region in the mean streamwise velocity field is observed in case 1 with the uniformly distributed foliage (i.e., the area encircled by the white line in Fig. 2). Such an in-canopy recirculation seems absent in both case 2 and case 3 in Fig. 2. As discussed in previous studies (e.g. Cassiani et al. 2008; Kanani-Sühring and Raasch 2017), the occurrence of an in-canopy recirculation is caused by the low-pressure zone in this region due to the vertical mass transport out of the forest. Looking closely at the occurrence frequencies of the negative streamwise velocity and streamlines of the flow in Fig. 3, however, the negative u events occur at a frequency of about 40% at about $x = 16h$ for case 2 and about 80% at about $x = 12h$ for case 1. This suggests that the foliage distributions regulate the locations and occurrence frequency of the in-canopy recirculation and the in-canopy recirculation has an unsteady and intermittent nature (Cassiani et al. 2008). For case 2, the time-averaged patterns shown in Fig. 2 smooth the in-canopy recirculation out to some extent showing a small positive u value near the edge (i.e., about 0.5 m s^{-1} at $x/h = 8$). The fairly low occurrence frequency (less than 10%) of the negative velocity downwind of the leading edge for case 3 suggests that the evidence is weak for an in-canopy recirculation to develop, likely due to the influence of the strong sub-canopy jet, as supported by the streamline pattern in Fig. 3b.

Besides these flow features, the influence of the vertical distributions of foliage on turbulence quantities are also identified in Fig. 2. For case 1 and case 2 with the relatively dense foliage in the lower-canopy part, all turbulence quantities (i.e., momentum flux, TKE, velocity skewness) exhibit quite similar patterns in their spatial variations even though an in-canopy recirculation does not appear in the mean-velocity field of case 2. Due to the much denser crown layer in case 3, a zone of large positive momentum flux and high TKE values develops below the crown layer immediately downwind of the edge as compared with case 1 and case 2, consistent with Dupont and Brunet (2008). Our analysis of the budget equation for the momentum flux (Eq. 3 in the Appendix) indicates that the positive momentum flux
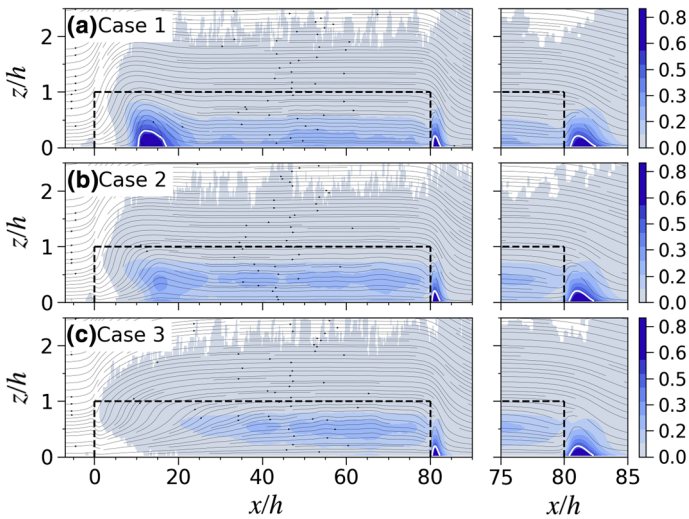
Fig. 3 Contour plots of negative streamwise velocity frequency, as denoted by the coloured areas scaling from 0 to 1 for the three cases with the different foliage distributions. Streamlines (thin black lines with arrow) are also plotted in this figure. The white lines represent the reversed flow region in the mean streamwise velocity fields. The leeside part is zoomed into highlight the differences (right panels)

within the canopy is largely attributed to the mean shear production term (i.e., $-w'w'\frac{\partial u}{\partial z}$), which is associated with the influence of the sub-canopy jet. This jet also causes the high in-canopy TKE zone downwind of the leading edge in case 3 (Dupont et al. 2012). This highly turbulent flow in case 3 is transported upwards to the canopy top as indicated by the positive vertical velocity in Fig. 2, and it then enhances turbulent mixing and reduces the enhanced gust zone as reflected by the region with the u skewness (SK_u) > 2.5 (Dupont and Brunet 2008).

In the leeside of the forest, these three foliage distributions lead to similar patterns in both the mean-velocity fields and the second- and third-order moments (Fig. 2). A small recirculation zone is detected in the mean streamwise velocity field for the three cases with a comparable size (Fig. 3), suggesting that the recirculation downwind of the leeside edge is insensitive to the foliage distributions, which differs from the in-canopy recirculation near the leading edge. This difference is probably attributed to the cleared ground and thus no drag forces exerted by canopy elements on flows. A small difference is observed in the TKE and momentum flux fields, though all are enhanced in the leeside as a result of the turbulent flux transport of these quantities down to this region. The influence of this leeside wake on turbulence can extend to a distance of 100 times the canopy height (Markfort et al. 2014). Such a leeside recirculation zone should have a great impact on scalar transport (Kanani-Sühring and Raasch 2017).

4 Influences of Edge Flows on Scalar Concentrations and Fluxes for Ground Sources

Two scalar source locations are designed to illustrate the influence of the three foliage distributions on scalar transport: the scalar source at the forested ground (i.e., from $x/h = 0$ to 80) and the cleared ground (i.e., $x/h < 0$ and $x/h > 80$). These two separate ground sources make

it possible to distinguish their contributions to concentration and fluxes with the identical flow fields. Both sources are set in a flux form rather than a concentration form and thus their contributions are additive. Note that the ground source is chosen primarily because it can illustrate the most pronounced features in the scalar field due to small wind speeds and turbulence near the surface, as indicated by Ross and Harman (2015) and Kanani-Sühring and Raasch (2015). For clarity, the scalar fields near the leading edge and in the leeside edge are discussed separately.

4.1 Scalar Transport with the Scalar Source Uniformly Distributed at the Forested Ground

Under the conditions with the horizontally uniform scalar source at the forested ground, strong concentration accumulations and large fluxes occur at about $x/h = 10$ for case 1 with a tall and narrow peak, and at about $x/h = 14$ for case 2 with a shallow and wide peak (Fig. 4). Apparently, the concentration peaks are associated with the streamwise flow convergences for these two cases. This statement is supported by case 3 without flow convergence and thus no corresponding concentration peak. The turbulent inflows for the three cases with the different foliage distributions are identical. The different persistence-lengths of the sub-canopy jets cause the different strengths of the streamwise flow convergences and thus different concentration peaks. Our analysis of the budget equation for scalar indicates that the advection terms are much larger than the turbulent transport terms, consistent with Kanani-Sühring and Raasch (2015). Note that the advection terms can be expressed in either the flux (i.e., $-u\frac{\partial C}{\partial x}$, where C represents scalar concentration) or advective (i.e., $-\frac{\partial uC}{\partial x}$) forms (Xue and Lin 2001), leading to different magnitudes although the net effect of advection as the sum of horizontal and vertical advection terms is the same. Previous studies have adopted both the flux (e.g., Ross and Harman 2015; Kanani-Sühring and Raasch 2015) and advective forms (e.g., Katul et al. 2006; Sogachev et al. 2008). Generally, the magnitudes of the individual terms in the flux form are smaller. Nevertheless, our results indicate that the horizontal and vertical advection terms dominate the scalar transport across the leading edge for the three cases no matter which form is used. Despite their importance, however, these advection terms cannot be captured by EC measurements.

The scalar flux field in Fig. 4 shows different features from the momentum flux field. It appears that the in-canopy recirculation has a large impact on the scalar flux while its impact on the momentum flux is minimal. As compared with the scalar concentration peaks, the flux peaks reach a height of at least $2h$. Our calculation with the scalar flux budget equation (i.e., Eq. 4 in the Appendix) indicates that the shear production term $-\overline{w'w'}\frac{\partial C}{\partial z}$ primarily contributes to the flux peaks, whereas the pressure term dominates the flux depletion, with the patterns of these two terms nearly identical to those of the scalar flux (figure not shown). For these three cases with a similar pattern in the $\overline{w'w'}$ fields, the different scalar flux distributions for the three cases are largely attributed to those in the concentration gradients which are primarily determined by the mean flow advection. As a consequence, the stronger flow convergence in case 1 leads to a high scalar flux peak with the position closer to the edge, as compared with that in case 2. The flow convergence is absent in case 3 with a long, strong sub-canopy jet which prevents the development of a flux peak.

These features can be illustrated in greater detail by comparing the scalar concentration and scalar flux at $0.3h$, $0.7h$, $1.0h$, and $1.5h$ (Fig. 5). Clearly, the foliage distributions lead to substantial changes in both the concentration and fluxes as x/h increases downwind of the leading edge. Abrupt jumps in both the concentration and fluxes occur at about $x/h = 10$
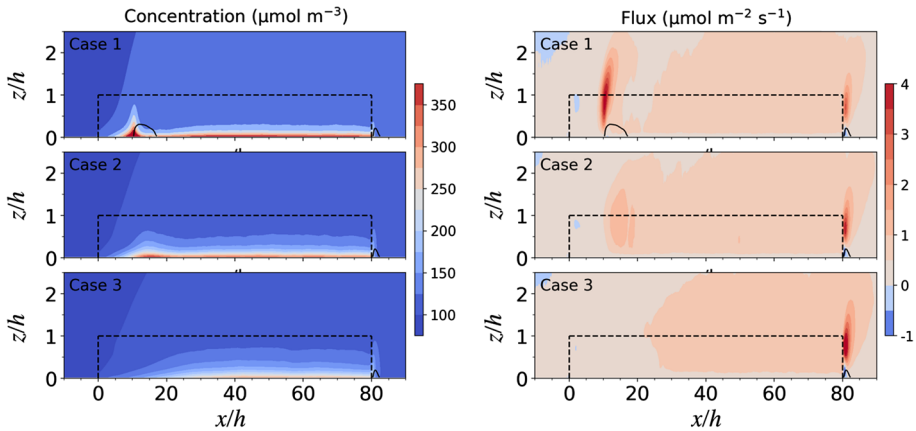
Fig. 4 Scalar concentrations (left) and fluxes (right) for the three cases with different foliage distributions. The scalar is released uniformly from the forest ground from $x/h = 0$ to 80

for case 1 and at about $x/h = 14$ for case 2 with the peaks associated with the in-canopy recirculation, whereas the situations are different for case 3 where the gentle increases with x/h are observed. In case 1 and case 2, the peak magnitudes for the concentration keep decreasing with height, whereas those for the flux increase from the ground to some height around $0.5h$, become nearly constant with height from $0.5h$ to $1.0h$ (the crown layer), and then decrease with height above $1.0h$. Also noticed is that the adjustment length before reaching an equilibrium and keeping constant with x/h for the concentration and flux both within and above the canopy is approximately $55h$, which is much longer than that for the momentum flux ($\approx 15h$), in line with the scaling arguments in Belcher et al. (2012). In other words, the edge effects are reduced to minimal at $x/h > 55$ for these three cases. Note that the equilibrium state of concentration/flux is defined as the same value that the three cases tend to reach. By this definition, the edge effect becomes minimal beyond this equilibrium distance. Considering the small fluctuations in the averaged results, the equilibrium distance is defined as the location where the concentration/flux reaches 95% of the equilibrium state.

The leeside edge effects are also identified by the links between the sudden changes in flux and concentration across the edge (Fig. 5). As discussed in the previous section, the nearly identical recirculation behind the leeside edge for the three cases indicates the small impacts of the different foliage distributions on the flows. Note that the leeside recirculation causes the small difference in the concentration gradient with height. The scalar fluxes at the different levels for the three cases, however, display large differences, with the highest peak value for case 3, followed by case 2, and then case 1, opposite to the flux peaks downwind of the leading edge. Overall, the small leeside recirculation mainly affects the near surface concentration, and its impact distance is limited to a few canopy heights ($\approx 3h$). Our analysis indicates that the shear production, $-\overline{w'w'}\frac{\partial C}{\partial z}$, in the flux budget equation is largely responsible for the flux difference downwind of the leeside edge (see Fig. 12 in the Appendix). The $\overline{w'w'}$ shows similar magnitudes for the three cases, but the $\frac{\partial C}{\partial z}$ has small differences (i.e., the large vertical scalar concentration gradient) above the leeside recirculation region due to the scalar concentration differences at the canopy crown layers in the equilibrium region. This small difference in the vertical concentration gradient is not evident in the concentration profiles in Fig. 5 due to the scale in the plots, but is responsible for the flux difference in the leeside. The largest flux as a result of the leeside edge effects is approximately located at the same
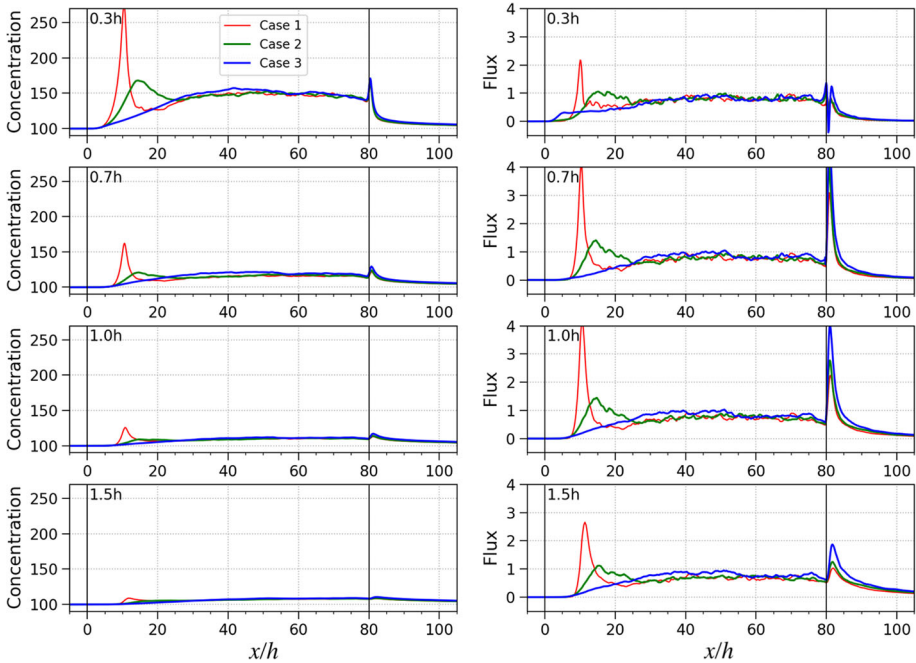
Fig. 5 Scalar concentrations in μmol m^{-3} (left panels) and the turbulent scalar flux in μmol m^{-2} s^{-1} (right panels) at $0.3h$, $0.7h$, $1.0h$, and $1.5h$. The scalar is released uniformly from the forested ground surface

height with the greatest leaf area density (*LAD*). The increased *LAD* value at the upper part of the canopy enhances the scalar flux in the leeside edge, opposite to the leading edge effect on the scalar flux (Fig. 5b). To study edge effects on fluxes peaks, measurements should be made at some distance downwind of the leading edge (e.g., $x/h = 10$–20 in our cases) and close to the leeside edge (e.g., $x/h = 2$ downwind of the leeside edge), depending on foliage distributions.

4.2 Scalar Transport with the Scalar Source Uniformly Distributed at the Cleared Ground

The scalar which is released uniformly from the cleared ground upwind of the leading edge (i.e., $x/h < 0$ in Fig. 6) provides a trace to illustrate how the scalar is transported by the edge flow into the canopy, which is then transported to the above-canopy atmosphere through the canopy crown layers, thereby contributing to the above-canopy flux. The scalar from the cleared ground is also transported following the streamline above the edge top, which directly contributes to the above-canopy flux. The relative contributions of these two processes to the above-canopy flux remain unknown. The accumulation of the scalar in the impact region before approaching the edge ($x/h = -1$) leads to the increased scalar concentration there (Fig. 6a). The distorted streamline and the elevated u and w zone above the canopy at $x/h = 0$ (Fig. 2) transport the scalar directly from the cleared ground to the canopy top, leading to the local flux maximum at about $x/h = 1.5$ despite the minimum concentration there (Fig. 6a, b). As x/h increases, the scalar fluxes for all the three cases decrease substantially until reaching its minimum at about $x/h = 3$ due to lack of the direct scalar transport from
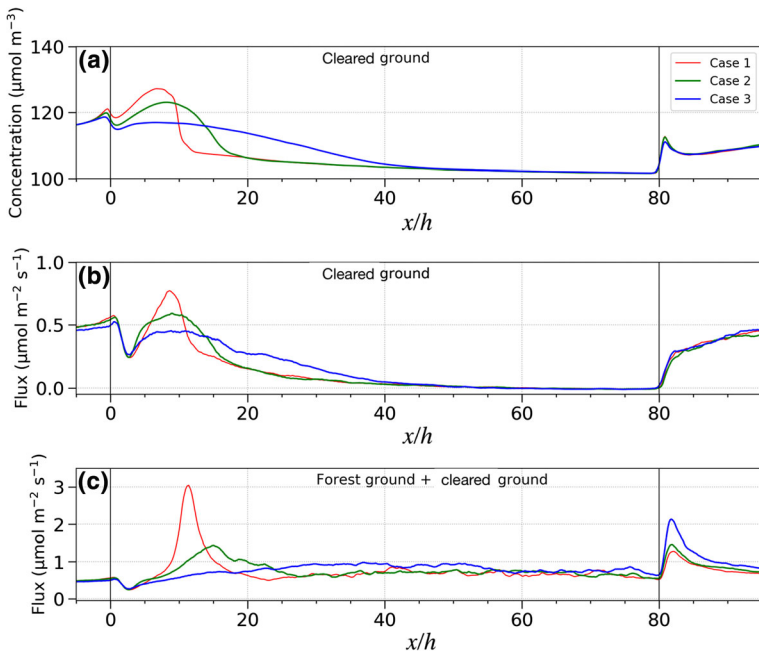
Fig. 6 a Scalar concentration at a height of 0.3*h*, and **b** turbulent scalar flux at a height of 1.5*h* under the scalar which is released uniformly from the cleared ground surface. The additive efforts of the scalar sources at the cleared ground and the forested ground on the flux at 1.5*h* is presented in panel c for comparison

the cleared ground. The buildup of the concentration downwind of the leading edge, which leads to a peak at about $x/h = 10$, is attributed to the decelerated flows and the damped turbulence due to the canopy elements (Dupont and Brunet 2009). As the distance from the edge increases, the increased within-canopy turbulence, particularly for case 1 and case 2 with the in-canopy recirculation, enhances the transport of the within-canopy scalar-rich air in the flow convergence zone out of the canopy, leading to the flux peaks above the canopy. Note that the above-canopy flux peak locations for case 1 and case 2 correspond to those of the strongest in-canopy recirculation. The much wider concentration peak for case 3 is primarily associated with the stronger sub-canopy jet that transfers the scalar farther downwind from the leading edge, resulting in the wider above-canopy flux peak than case 1 and case 2. Despite the abrupt drops in both the concentration and flux for case 1 and case 2 with the increased x/h, the equilibrium length is about 40*h* where both the concentration and flux reach their background values (Figs. 6a, b). However, the impact length of the scalar flux for the cleared ground-surface source (approximately $x/h = 40$) is shorter than that for the forested ground-surface source (approximately $x/h = 55$). Therefore, due to the additive effect, the above-canopy flux does not reach its equilibrium until approximately $x/h = 55$ under the influence of both the cleared ground sources and forested ground sources (Fig. 6c). However, it is found that the scalar source at the forested ground dominates the contribution to the above-canopy flux (note the scale difference in Fig. 6b, c).

By examining the scalar flux budget, it is found again that the shear production $-\overline{w'w'}\frac{\partial C}{\partial z}$ contributes most to the above-canopy flux. Caused by the streamwise flow convergence, case 1 has the largest scalar gradient $\frac{\partial C}{\partial z}$, explaining the largest flux peak, followed by case 2 and case 3. This peak appears roughly at the same location as that for the forested ground source

(Fig. 6b). Our tests indicate that the scalar flux for the cleared ground source is independent of wind speeds, consistent with Kanani-Sühring and Raasch (2015).

Both the concentration and flux downwind of the leeside edge have almost identical variation patterns for all the three cases, indicating that the vertical foliage distributions have minimal impacts on the scalar flux with the cleared ground source. Given the near-zero scalar fluxes and the same background concentrations for the inflow from the forest (i.e., from x/h = 60 to 80) for three cases, the fairly similar flow dynamics and the associated recirculation behind the leeside edge result in a nearly identical above-canopy scalar flux.

5 Scalar Transport with the Scalar Sources in the Different Canopy Layers

Figure 7 shows the scalar flux at a height of 1.5h for each case with identical flow dynamics but with three different scalar sources located in the three heights of the canopy layers (0.3h, 0.6h, and 0.9h). One noticeable feature for each case is that with decreasing source height, variations in flux with x/h are more pronounced, consistent with Ross and Harman (2015). This is primarily due to small wind speeds and thus less turbulent mixing within the lower canopy layers thereby resulting in local accumulation of scalar concentration and large gradients. As a consequence, the large concentration gradients yield the large scalar flux at the canopy top given nearly the same $\overline{w'w'}$ in the term $-\overline{w'w'}\frac{\partial C}{\partial z}$. Note that since the flow convergence is mainly located at the lower canopy part and the convergence is fairly weak at the upper canopy layers, the small concentration gradients in the upper canopy layers lead to the collapsed patterns in the scalar fluxes for the three cases when the sources are set at the upper canopy layers. In case 3 without a flow convergence, the within-canopy flow is primarily regulated by the strong sub-canopy jet, which is expected to have less impact on the sources closer to the canopy top. Also noticed in Fig. 7 is that all the scalar fluxes reach the equilibrium value approximately at x/h = 30 for all three cases with sources above the ground. Our results suggest that to avoid the edge effects, measurements should be made at least x/h >30 from the leading forest edge under the influence of canopy scalar sources.

Similar to the leading edge, the magnitudes of the flux peaks across the leeside edge increase with decreasing source height, due to the influence of the small recirculation in the lee. When the scalar sources are located in the upper layers of the canopy, the small recirculation has relatively less impact on the fluxes and produces no flux peaks (i.e., 0.6h and 0.9h for both case 1 and case 2). These results suggest that the leeside flux peaks do not necessarily occur, largely depending on scalar source locations.

6 Simulations with Scalar Sources Generated from the Multiple-Layer Canopy Model

In this section, CO_2 and water vapour sources/sinks in the canopy are simulated using the MCANOPY module (Ma and Liu 2019) to investigate the edge effects on the CO_2 concentration, specific humidity, and on the CO_2 and water vapour fluxes. The soil respiration rate is set to be 5.5 μmol m^{-2} s^{-1} from both the cleared and forested ground surfaces, a rate close to that from field measurements (Patton et al. 2011). The numerical configurations and the three foliage distributions are identical to those in the previous sections. Neutral atmospheric conditions are considered for this case study to exclude stability effects to highlight the influ-
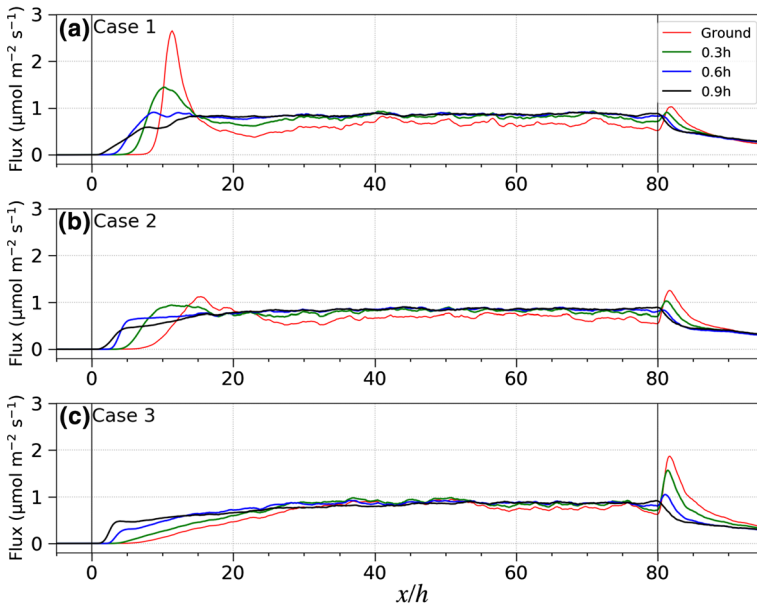
Fig. 7 Turbulent scalar flux at a height of $1.5h$ for case 1 (**a**), case 2 (**b**), and case 3 (**c**). Scalar sources are located in the three different canopy layers of $0.3h$, $0.6h$, and $0.9h$. The results for the scalar sources at the forested ground are also plotted in this figure for comparison

ence of flow dynamics, although the MCANOPY module is capable of studying stability effects (Ma and Liu 2019). The neutral stability condition is set by using a constant potential temperature in the domain, where the water vapour thermodynamic effect is excluded. As indicated in Figs. 8 and 9, the CO_2 concentration and specific humidity and their fluxes show remarkably different fields due to the different locations for their corresponding sources and sinks. As shown in Figs. 8 and 9, the CO_2 sources (respiration) are primarily located on the soil surface, and the sinks (photosynthesis) in the upper canopy layer, while the water vapour sources are primarily from evaporation located at the upper layers of the canopy and from the cleared ground. It is expected that CO_2 concentration is generally greater closer to the ground surface. A high CO_2 concentration zone is observed downwind of the leading edge in case 1 and case 2 as a combined effect of the flow convergence associated with the recirculation and the horizontal inflow with CO_2-riched air masses from the upwind cleared soil surface. Due to the deep, sparse trunk space in case 3 with the strong sub-canopy jet, such a strong high concentration zone does not occur. The relatively strong turbulence associated with the sub-canopy jet in the sparse trunk space in case 3 creates a large zone with high CO_2 concentration and thus large CO_2 flux. Another noticeable feature is the triangle shaped patterns of low CO_2 concentration for the three cases; such low concentration regions start at the leading edge and show a progressively decreased CO_2 concentration centred in the crown layer as a result of the elevated CO_2 concentration near the surface, the low CO_2 concentration in the upwind flow from the cleared ground, and the reduced CO_2 concentration caused by photosynthesis (the left panels in Fig. 8). Our results indicate that those spatial variations in CO_2 fluxes both above and within the canopy are primarily associated with those in CO_2 concentration (the middle panels in Fig. 8). It should be mentioned that for the three cases, the sink rate of CO_2 is about $-26\ \mu\text{mol m}^{-2}\ \text{s}^{-1}$, which is about five times the ground
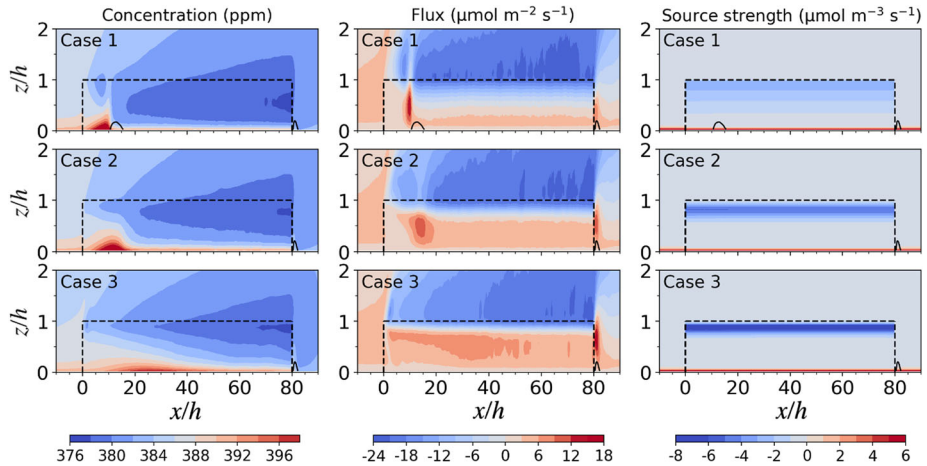
Fig. 8 Spatial variations in CO_2 concentration (left), CO_2 flux (middle), and the CO_2 sources/sinks (right) as simulated by the MCANOPY module
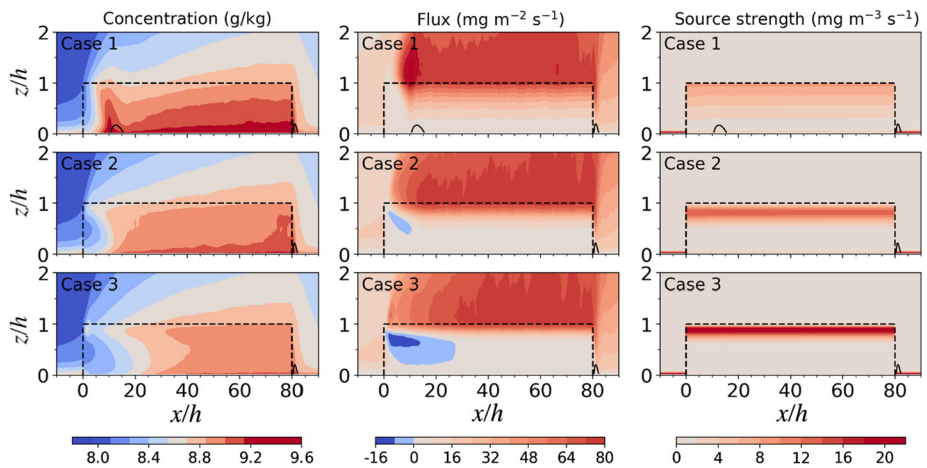

Fig. 9 Spatial variations in specific humidity concentration (left), water vapour flux (middle), and the water vapour sources/sinks (right) as simulated by the MCANOPY module

source rate. However, the concentration accumulation is still observed for case 1 and case 2, suggesting the influence of the source/sink distributions.

Both the canopy layer and the soil surface act as water vapour sources via transpiration and evaporation, respectively. The spatial variations in the specific humidity and water vapour flux in Fig. 9 show the substantially different patterns from those for CO_2 in Fig. 8 with the identical flow dynamics mainly due to the different source locations between specific humidity and CO_2. A noticeable feature is that a strong accumulation zone downwind of the leading edge is observed for case 1 but not for case 2 and case 3, largely attributable to the source differences. This accumulation also causes a high flux zone at the top of the canopy for case 1 only. The low (or negative) flux zone downwind of the leading edge within the canopy for case 2 and case 3 results from the intrusion of the air masses with low water
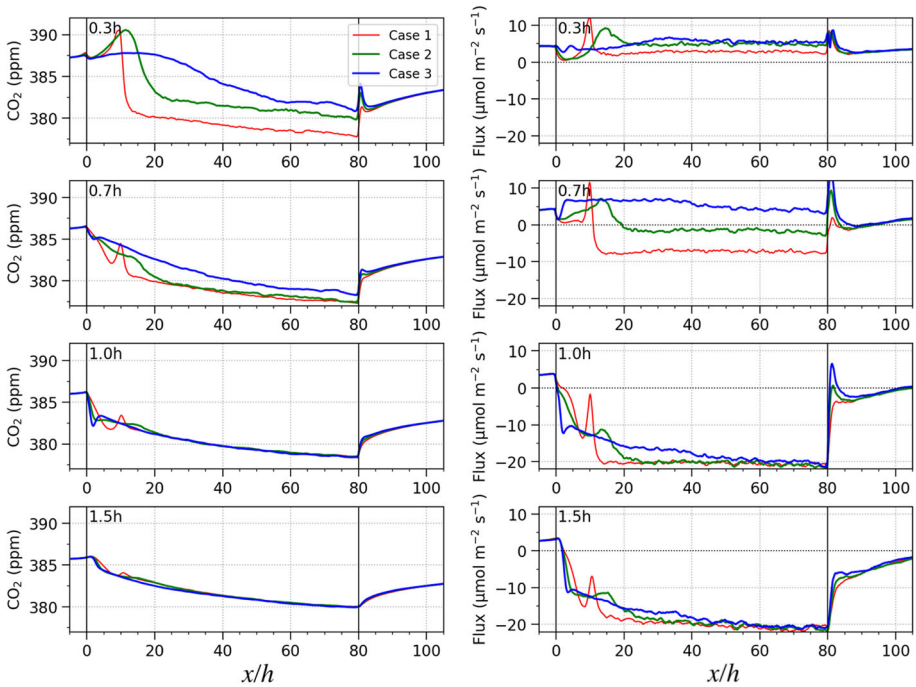
Fig. 10 CO_2 concentration (left panels) and CO_2 fluxes (right panels) at $0.3h$, $0.7h$, $1.0h$, and $1.5h$ for the three cases. The CO_2 and water vapour sources/sinks are produced by the MCANOPY module

vapour concentration from the upwind cleared ground. The above-canopy water vapour flux also shows large spatial variations with height and distance from the leading edge. Another noticeable feature is the small negative water vapour fluxes near the leading edge for case 2 and case 3 (the middle panels in Fig. 9), indicating a downward water vapour transport. This unique feature is caused by the high specific humidity at the canopy top and the low specific humidity at the lower layers as a result of the low specific humidity in the upwind flow from the cleared ground and the large source near the canopy top. From Figs. 8 and 9, the scalar concentration and flux distributions are much more complicated near the forest leading edge (i.e., $x/h < 20$h), where the scalar concentration and flux patterns are greatly influenced by a combination of the inflow concentration from the cleared ground, the forested ground source/sink strength, and the canopy layer source/sink strength.

The influences of foliage distributions on both scalar concentration and fluxes are also reflected by their variations with x/h at different heights for the three cases (Figs. 10, 11). The largest differences in scalar concentrations among the three cases occur in the lower part of the canopy (e.g., $0.3h$ followed by $0.7h$) due to the low wind speeds and thus reduced mixing deep in the canopy, whereas the largest differences in fluxes occur in the upper part of the canopy (e.g., $0.7h$ followed by $0.3h$) particularly for $x/h < 20$ resulting from the horizontal flux convergence. The smallest differences in both the concentration and flux are observed above the canopy, and they become even negligibly small for $x/h > 20$ for CO_2 concentration, $x/h = 60$–80 and $x/h > 90$ for CO_2 flux, $x/h > 20$ for specific humidity, and $x/h > 30$ for water vapour flux. Under the given source conditions, both the CO_2 concentration and specific humidity above the canopy never reach an equilibrium as x/h increases, but the CO_2 flux reaches its equilibrium at a larger distance of about $x/h = 60$ compared to the water vapour
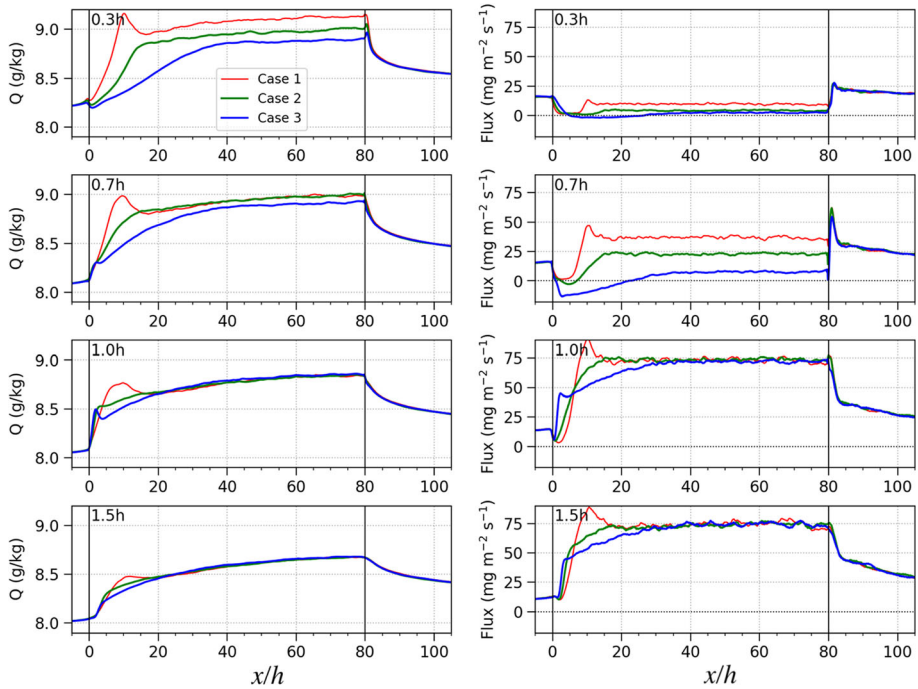
Fig. 11 Specific humidity (left) and water vapour fluxes (right) at $0.3h$, $0.7h$, $1.0h$, and $1.5h$ for the three cases. The CO_2 and water vapour sources/sinks are produced by the MCANOPY module

flux which reaches equilibrium at about $x/h = 30$. This result suggests that the CO_2 flux at $z/h = 1.5$ above the canopy requires a much longer distance from the leading edge to reach an equilibrium than the water vapour flux (Figs. 10 vs. 11). This is caused by the distribution difference in the concentration field, which then causes the difference in shear production term that dominates in the flux budget (see Fig. 12 in the Appendix). To avoid this edge effect, our "real" case simulations suggest that any CO_2 flux measurements over finite size forests with edges should be located further downwind from the leading edge than previously estimated since most of the previous studies have used idealized distributions of CO_2 sources/sinks (e.g., Kanani-Sühring and Raasch 2015).

7 Conclusions

Forest-edge flows and associated scalar transfer were investigated using the WRF–LES model and a newly developed multiple-layer canopy module (MCANOPY) by considering the influence of the vertical distributions in foliage and scalar sources/sinks. The most noticeable flow convergence, which develops within the canopy downwind of the leading edge for the relatively uniformly distributed foliage, is not observed in the canopy with a deep, sparse trunk space due to the presence of a strong sub-canopy jet. As expected, the sub-canopy layers below the crown experience the most significant impacts from the leading edge, leading to the distinct flow dynamics in this region and thus scalar transfer. This flow convergence leads to the within-canopy concentration maximum and thus a large vertical concentration gradient for case 1 and case 2. Due to the above-canopy TKE maximum which appears right

above the within-canopy concentration maximum, an above-canopy flux peak occurs no matter where the scalar sources are located. This feature does not occur for case 3, reflecting the influence of the foliage distributions. Also attributed to these distinct flow dynamics in the sub-canopy layer, the dynamical flows have more significant effects on scalar sources located on the ground surface and in the lower parts of the canopy. The spatially-distributed scalar sources/sinks on the forested ground surface, the cleared ground, and in the canopy layers make the scalar concentration and flux fields more complicated as simulated by the MCANOPY module in a more realistic case. Both the concentration and flux fields are highly dynamical within and above the canopy. At the leeside edge, a small recirculation also develops and has consistent features for the three foliage distributions.

Our results indicate that the scalar flux at a height of $1.5h$ requires much longer distance from the edge to reach its equilibrium (about $x/h = 30$) than previously thought. This adjustment distance is even longer with real sources/sinks to avoid the edge effect for eddy-covariance flux measurements over the canopy. Therefore, assessing source distribution and canopy structures is necessary for locating flux towers over finite size forests with edges.

Appendix: Flux Budget Equations Over a Forest Edge

Assuming neutral stratification, steady-state flow, homogeneity in the spanwise direction, and ignoring the subgrid-scale contribution (Stull 2012), the budget equation for the resolved-scale momentum flux $u'w'$ can be written as

$$\frac{\partial u'w'}{\partial t} = 0 = -u\frac{\partial u'w'}{\partial x} - w\frac{\partial u'w'}{\partial z} \tag{3a}$$

$$-u'w'\frac{\partial w}{\partial z} - u'u'\frac{\partial w}{\partial x} - u'w'\frac{\partial u}{\partial x} - w'w'\frac{\partial u}{\partial z} \tag{3b}$$

$$-\frac{\partial w'u'u'}{\partial x} - \frac{\partial w'w'u'}{\partial z} \tag{3c}$$

$$-\frac{1}{\rho}\left(w'\frac{\partial p'}{\partial x} + u\frac{\partial p'}{\partial z}\right). \tag{3d}$$

The terms on the right-hand side of Eq. 3 represent, respectively, advection by the mean flow (3a), shear production by the velocity gradient (3b), flux transported by turbulent motions (3c), and pressure re-distribution effect (3d).

Similarly, for any scalar c (e.g., CO_2), the resolved-scale scalar flux $w'c'$ can be written as

$$\frac{\partial w'c'}{\partial t} = 0 = -u\frac{\partial w'c'}{\partial x} - w\frac{\partial w'c'}{\partial z} \tag{4a}$$

$$-w'c'\frac{\partial w}{\partial z} - u'c'\frac{\partial w}{\partial x} \tag{4b}$$

$$-w'u'\frac{\partial c}{\partial x} - w'w'\frac{\partial c}{\partial z} \tag{4c}$$

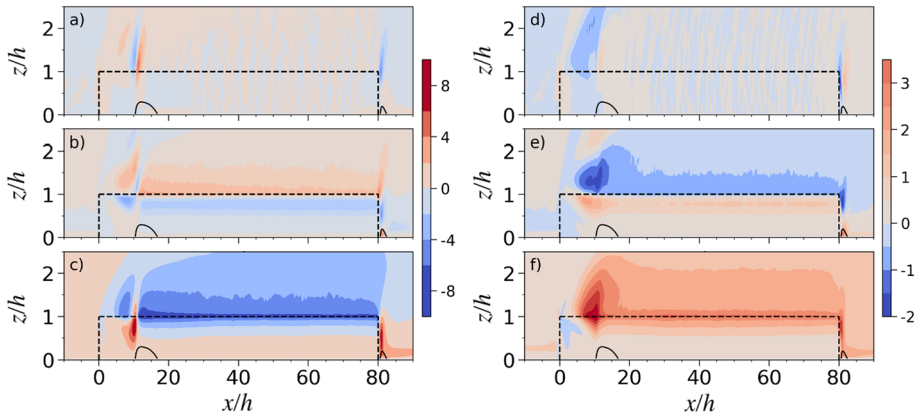$$-\frac{\partial w'u'c'}{\partial x} - \frac{\partial w'w'c'}{\partial z} \tag{4d}$$

Fig. 12 Spanwise- and time-averaged scalar flux balance terms for case 1, CO_2 flux (left) and water vapour fluxes (right). **a** and **d** advection by the mean flow, **b** and **e** flux transported by turbulent motions, **c** and **f** shear production for CO_2 and water vapour fluxes, respectively. All terms are normalized by $\frac{h}{u_*^2 C_*}$ for CO_2 and $\frac{h}{u_*^2 Q_*}$ for water vapour fluxes, where u_* is the canopy-top friction velocity. Parameters C_* and Q_* are CO_2 and specific humidity scales defined as the canopy-top fluxes divided by u_*. All the three parameters are deduced at $x/h = 60$ and $z/h = 1$

$$-\frac{1}{\rho}\left(\frac{\partial p' c'}{\partial z} - p' \frac{\partial c'}{\partial z}\right). \tag{4e}$$

The terms on the right-hand side of Eq. 4 represent, respectively, advection by the mean flow (4a), shear production by the velocity gradient (4b), shear production by the scalar gradient (4c), flux transported by turbulent motions (4d), the pressure re-distribution effect (4e).

Figure 12 shows the three terms in the CO_2 and water vapour flux budget for case 1 (uniformly distributed *LAI*). All the terms are normalized in this figure.

References

Belcher SE, Jerram N, Hunt JCR (2003) Adjustment of a turbulent boundary layer to a canopy of roughness elements. J Fluid Mech 488:369–398

Belcher SE, Harman IN, Finnigan JJ (2012) The wind in the willows: flows in forest canopies in complex terrain. Annu Rev Fluid Mech 44:479–504

Bonan GB (2008) Forests and climate change: forcings, feedbacks, and the climate benefits of forests. Science 320:1444–1449

Bou-Zeid E, Meneveau C, Parlange M (2005) A scale-dependent Lagrangian dynamic model for large eddy simulation of complex turbulent flows. Phys Fluids 17:025105

Cassiani M, Katul GG, Albertson JD (2008) The effects of canopy leaf area index on airflow across forest edges: large-eddy simulation and analytical results. Boundary-Layer Meteorol 126:433–460

Dupont S, Brunet Y (2008) Edge flow and canopy structure: a large-eddy simulation study. Boundary-Layer Meteorol 126:51–71

Dupont S, Brunet Y (2009) Coherent structures in canopy edge flow: a large-eddy simulation study. J Fluid Mech 630:93–128

Dupont S, Bonnefond JM, Irvine MR, Lamaud E, Brunet Y (2011) Long-distance edge effects in a pine forest with a deep and sparse trunk space: in situ and numerical experiments. Agric For Meteorol 151:328–344

Dupont S, Irvine MR, Bonnefond JM, Lamaud E, Brunet Y (2012) Turbulent structures in a pine forest with a deep and sparse trunk space: stand and edge regions. Boundary-Layer Meteorol 143:309–336

Foken T, Serafimovich A, Eder F, Hübner J, Gao Z, Liu H (2017) Interaction forest–clearing. In: Foken T (ed) Energy and matter fluxes of a spruce forest ecosystem, vol 229. Springer, Berlin, pp 309–329

Kanani F, Traeumner K, Ruck B, Raasch S (2014) What determines the differences found in forest edge flow between physical models and atmospheric measurements? An LES study. Meteorol Z 23:33–49

Kanani-Sühring F, Raasch S (2015) Spatial variability of scalar concentrations and fluxes downstream of a clearing-to-forest transition: a large-eddy simulation study. Boundary-Layer Meteorol 155:1–27

Kanani-Sühring F, Raasch S (2017) Enhanced scalar concentrations and fluxes in the lee of forest patches: a large-eddy simulation study. Boundary-Layer Meteorol 164:1–17

Kanani-Sühring F, Falge E, Voß L, Raasch S (2017) Complexity of flow structures and turbulent transport in heterogeneously forested landscapes: large-eddy simulation study of the Waldstein site. In: Foken T (ed) Energy and matter fluxes of a spruce forest ecosystem. Ecological Studies (Analysis and Synthesis), vol 229

Katul GG, Finnigan JJ, Poggi D, Leuning R, Belcher SE (2006) The influence of hilly terrain on canopy-atmosphere carbon dioxide exchange. Boundary-Layer Meteorol 118:189–216

Klaassen W, van Breugel PB, Moors EJ, Nieveen JP (2002) Increased heat fluxes near a forest edge. Theor Appl Climatol 72:231–243

Kröniger K, Banerjee T, De Roo F, Mauder M (2017) Flow adjustment inside homogeneous canopies after a leading edge—an analytical approach backed by LES. Agric For Meteorol 255:17–30

Ma Y, Liu H (2017) Large-eddy simulations of atmospheric flows over complex terrain using the immersed-boundary method in the weather research and forecasting model. Boundary-Layer Meteorol 75:1–25

Ma Y, Liu H (2019) An advanced multiple-layer canopy model in the Weather Research and Forecasting (WRF) model with large-eddy simulations to simulate canopy flows and scalar transport under different stability conditions. J Adv Model Earth Syst. https://doi.org/10.1029/2018MS001347

Markfort CD, Porté-Agel F, Stefan HG (2014) Canopy-wake dynamics and wind sheltering effects on Earth surface fluxes. Environ Fluid Mech 14:663–697

Oldroyd HJ, Katul G, Pardyjak ER, Parlange MB (2014) Momentum balance of katabatic flow on steep slopes covered with short vegetation. Geophys Res Lett 41:4761–4768

Oleson K, Lawrence M, Bonan B, Drewniak B, Huang M, Koven D, Levis S, Li F, Riley W, Subin Z, Swenson S, Thornton P (2013) Technical description of version 4.5 of the Community Land Model (CLM)

Patton EG, Horst TW, Sullivan PP, Lenschow DH, Oncley SP, Brown WO, Burns SP, Guenther AB, Held A, Karl T, Mayor SD (2011) The canopy horizontal array turbulence study. Bull Am Meteorol Soc 92(5):593–611

Porté-Agel F, Meneveau C, Parlange MB (2000) A scale-dependent dynamic model for large-eddy simulation: application to a neutral atmospheric boundary layer. J Fluid Mech 415:261–284

Ross AN, Baker TP (2013) Flow over partially forested ridges. Boundary-Layer Meteorol 146:375–392

Ross AN, Harman IN (2015) The impact of source distribution on scalar transport over forested hills. Boundary-Layer Meteorol 156:211–230

Schlegel F, Stiller J, Bienert A, Maas H-G, Queck R, Bernhofer C (2012) Large-eddy simulation of inhomogeneous canopy flows using high resolution terrestrial laser scanning data. Boundary-Layer Meteorol 142:223–243

Shaw RH, Schumann U (1992) Large-eddy simulation of turbulent flow above and within a forest. Boundary-Layer Meteorol 61:47–64

Skamarock W, Klemp J, Dudhia J, Gill D, Barker D, Duda M, Huang X, Wang W, Powers J (2008) A description of the advanced research WRF version 3. NCAR, Boulder

Sogachev A, Leclerc MY, Zhang G, Rannik Ü, Vesala T (2008) CO_2 fluxes near a forest edge: a numerical study. Ecol Appl 18:1454–1469

Stull RB (2012) An introduction to boundary layer meteorology, vol 13. Springer, Berlin

Xue M, Lin SJ (2001) Numerical equivalence of advection in flux and advective forms and quadratically conservative high-order advection schemes. Mon Weather Rev 193:561–565

Yang B, Raupach MR, Shaw RH, Morse AP (2006) Large-eddy simulation of turbulent flow across a forest edge. Part I: flow statistics. Boundary-Layer Meteorol 120:377–412

Yi C (2008) Momentum transfer within canopies. J Appl Meteorol Clim 47:262–275

Yi C, Pendall E, Ciais P (2015) Focus on extreme events and the carbon cycle. Environ Res Lett 10:70201–70208